Journal of Biomechanics 113 (2020) 110087

Contents lists available at ScienceDirect

Journal of Biomechanics

journal homepage: www.elsevier.com/locate/jbiomech
www.JBiomech.com

Development of a neural network based control algorithm for powered ankle prosthesis

A. Doğukan Keleş, Can A. Yucesoy *

Biomedical Engineering Institute, Boğaziçi University, Istanbul, Turkey

ARTICLE INFO

Article history:
Accepted 16 October 2020

Keywords:
Powered ankle prosthesis
Neural networks
Transtibial amputation
Ankle disarticulation
sEMG

ABSTRACT

Lower limb amputation is partial or complete removal of the limb due to disease, accident or trauma. Surface electromyograms (sEMG) of a large number of muscles and force sensors have been used to develop control algorithms for lower limb powered prostheses, but there are no commercial sEMG controlled prostheses available to date. Unlike ankle disarticulation, transtibial amputation yields less intact lower leg muscle mass. Therefore, minimizing the use of sEMG muscle sources utilized will make powered prosthesis controller *economic*, and limiting the use of specifically the lower leg muscles will make it *flexible*. Presently, we have used healthy population data to (1) test the feasibility of the neural network (NN) approach for developing a powered ankle prosthesis control algorithm that successfully predicts sagittal ankle angle and moment during walking using exclusively sEMG, and (2) rank all muscle combination variations according to their success to determine the economic and flexible NN's. sEMG amplitudes of five lower extremity muscles were used as inputs: the tibialis anterior (TA), medial gastrocnemius (MG), rectus femoris (RF), biceps femoris (BF) and gluteus maximus (GM). A time-delay feed-forward-multilayer-architecture NN algorithm was developed. Muscle combination variations were ranked using Pearson's correlation coefficient ($r > 0.95$ indicates successful correlations) and root-mean-square error between actual vs. estimated ankle position and moment. The trained NN TA + MG was successful ($r_{position} = 0.952$, $r_{moment} = 0.997$) whereas, TA + MG + BF ($r_{position} = 0.981$, $r_{moment} = 0.996$) and MG + BF + GM ($r_{position} = 0.955$, $r_{moment} = 0.995$) were distinguished as the economic and flexible variations, respectively. The algorithms developed should be trained and tested for data acquired from amputees in new studies.

1. Introduction

Recent technological developments particularly on embedded computing, sensors, and batteries have advanced the field of assistive robotics to restore legged locomotion for individuals suffering from lower limb amputations (Lawson et al., 2014). First examples of assistive devices were energy storing and return prosthetics, which provided a great improvement over purely passive prostheses with and without joints and are being used successfully, still dominating the commercial lower limb prostheses currently available. Owing to their relative simplicity, low cost, and robust design, these devices are practical tools to enable functional recovery of gait pathologies stemming from several conditions. Passive-elastic energy storage and return ankle prostheses restore some ankle function, but especially in fast walking external energy input is necessary to achieve close to normal gait patterns. Their inherent shortcomings include inability to generate positive mechanical power and lacking autonomous adaptation to the user's changing needs (Gates et al., 2004; Palmer, 2002; Tucker et al., 2015).

Recently, powered prostheses have been developed to assist normal gait beyond slow walking speeds (Culver et al., 2018; Hargrove et al., 2015; Spanias et al., 2018). Surface electromyograms (sEMG) assist the prediction of joint position and moment changes (Hoozemans and Van Dieën, 2005; Jephil et al., 2020), and are used to control assistive robotic systems (Al-Quraishi et al., 2015; Cavallaro et al., 2006; Fleischer and Hommel, 2008; Spanias et al., 2015). Biomimetic models, neural networks, fuzzy logic and genetic algorithms are used for sEMG classification (Naidu et al., 2008). Sepulveda et al. (1993) developed a neural network with the back-propagation algorithm to model the relationship between muscle activity and joint motion. Note that, sEMG is influenced by noise due to, e.g., cross talk, changes in skin conductivity, and artifacts originating from, e.g., movement at the skin-electrode interface and signal amplifiers (De Luca et al.,

* Corresponding author at: Biomedical Engineering Institute, Boğaziçi University, 34684, Çengelköy, Istanbul, Turkey.
E-mail address: can.yucesoy@boun.edu.tr (C.A. Yucesoy).

https://doi.org/10.1016/j.jbiomech.2020.110087
0021-9290/

2010). As the condition of the remaining lower leg muscles strongly depends on the type of amputation surgery performed and the trauma experienced, the sEMG signal quality varies from patient to patient. Unlike in ankle disarticulation, which does not interfere with lower leg muscles, less lower leg muscle mass remains intact in transtibial amputation. Moreover, amputation level in transtibial amputations differs among patients being performed near the knee or closer to the ankle. Therefore, minimizing the number of sEMG muscle sources utilized will make powered prosthesis controller *economic*, and limiting the use of specifically the lower leg muscles will make it *flexible* ideally for both ankle disarticulation and transtibial amputation. However, for predicting position and moment changes in lower extremity joints via sEMG, Sepulveda et al. (1993) used 16 muscles involving six lower leg muscles including extensor digitorum longus, peroneus longus, tibialis anterior, medial gastrocnemius, lateral gastrocnemius and soleus. Similarly, Zhang et al. (2010) used five of those muscles to control an ankle exoskeleton (excluding the extensor digitorum longus). Au et al. (2008) used additional force feedback to the sEMG of tibialis anterior, medial gastrocnemius and lateral gastrocnemius to accurately estimate joint position however, the additional sensors required increase device cost and weight. Fleischer and Hommel, (2008) utilized six upper leg muscles, but also force feedback, whereas Sup et al. (2008) eliminated sEMG by using three force sensors instead. Therefore, current control algorithms for powered ankle prosthesis utilize either a large number of sEMG sensors involving numerous lower leg muscles or several force sensors, or a combination. Development of a low-cost, user-friendly assistive powered ankle prosthetic device requires a flexible control algorithm, which can minimize sEMG sensors, reduce the need for lower leg muscles, while avoiding force sensors.

The aims using healthy population data were to (1) test the feasibility of the neural network (NN) approach for developing powered ankle prosthesis control algorithm that successfully predicts real-time sagittal ankle angle and moment during walking using exclusively lower limb sEMG, and (2) rank all muscle combination variations according to their success to determine the economic and flexible NN's.

2. Methods

2.1. Dataset

Gait data are required for developing, training, and testing NNs. For that purpose, sEMG amplitudes, sagittal ankle angle, and moment of walking trials were acquired from the open database by Bovi et al. (2011). In this database, data from forty able-bodied subjects were classified into two age groups: young (9 males, 11 females, 6–17 years, mean (SD) 10.8 (3.2) years, body height 1.47 (0.20) m) and adult (9 males, 11 females, 22–72 years, mean (SD) 43.1 (15.4) years, body height 1.71 (0.10) m). The subjects walked over level ground at a *self-selected speed* (normalized for body height (BH): adult 71.4 ± 10.2 and young 87.7 ± 15.8 %BH/s), and faster speeds (v) classified as *very slow* (v/BH < 0.6), *slow* (0.6 ≤ v/BH < 0.8), *medium* (0.8 ≤ v/BH < 1), and *fast* (v/BH > 1). Mean data of three trials per each speed were utilized.

sEMG data of tibialis anterior (TA), medial gastrocnemius (MG), rectus femoris (RF), biceps femoris (BF) and gluteus maximus (GM) were recorded unilaterally on the dominant side with electrode locations in agreement with SENIAM (Hermens et al., 2000). In a recent work by the same group (Lencioni et al. 2019), specifics of the sEMG acquisition were described: self-adhesive Ag-AgCl electrodes (Medtronic Kendall, USA, 24 mm electrode diameter, 10 mm active part diameter, bipolar configuration, 20 mm inter-electrode distance) were used and sEMG data were band-pass filtered (10–400 Hz) before sampling to reduce the aliasing effect. Bovi et al. (2011) applied rectification and low-pass filtering (Butterworth 5th order, 3 Hz cutoff frequency). Additionally, sEMG data for each subject's channel individually was normalized for the maximum of the root mean square values of 2% intervals across each trial. Joint moments calculated using simultaneously collected gait data (SMART-E motion capture system, BTS, Italy utilizing total-body LAMB marker set and force plates, Kistler, Switzerland) were normalized by body mass. Data for each speed class per age group were averaged yielding a total of 10 datasets for further analyses.

2.2. Neural network development

All NNs developed feature the following: (1) A time delay feed-forward multilayer NN architecture was used. This enables the networks to generate sEMG based continuous estimation of joint kinematics based on time-varying inputs (Liu et al., 2017; Rahmatian et al., 2016) and capability of accounting for the delay between onset of EMG activity and mechanical movement (Pulliam et al., 2011). (2) In addition to an input and an output layer, one hidden layer was used. This was shown to be sufficient for joint movement predictions (Liu et al., 2017; Rahmatian et al., 2016). The hidden layer has 32 neurons with a nineteen-data-tapped delay. This was determined as the outcome of a systematical variation of the number of neurons and the time delay between 5-50 and 5–20, respectively yielding the highest correlations for ankle position and moment changes in the sagittal plane for five sEMG inputs. For each NN, a sigmoidal transfer function was used in the hidden layer. The number of neurons in the input layer varies according to the number of sEMG inputs. In the output layer, a linear transfer function was used so that the neural outputs could take on any value. A basic representation of the NN structure developed is shown in Fig. 1A.

In order to predict the ankle position and moment, sEMG amplitudes of the following five lower extremity muscles were used as NN inputs: the TA and MG in the lower leg and the RF, BF and GM in the upper leg. To test the success of NN variations all possible muscle combinations were studied (in total 31: 5 single, 10 two, 10 three, 5 four and 1 five muscle combinations).

The best-performing variations including (i) the minimum total number of muscle inputs and (ii) smallest number of lower leg muscles were sought after. The former is referred to as the *economic variation* and the latter representing applicability for both amputation levels is referred to as the *flexible variation*. A variation including only upper leg muscles is classified as *ideally flexible*.

2.3. Neural network training

2.3.1. Main and versatility implementations

The dataset involving five speed classes was split into training (four speed classes) and test (the remaining one speed class) datasets. The testing was first conducted on the *main implementation*: datasets for very slow, slow, medium and fast speed classes were used in NN training, whereas those for self-selected speed class were used for testing. This was used to evaluate all NN variations. Subsequently on the economic and flexible variations determined, *versatility implementations* were tested: for each of very slow, slow, medium and fast speed classes assessed for implementation, the remaining speed classes were used as training datasets (Table 1).

2.3.2. Data augmentation

Per each speed class, sEMG data of both young and adult groups were averaged per muscle. Therefore, out of the 10 datasets, a total of 8 training datasets were available for each implementation.

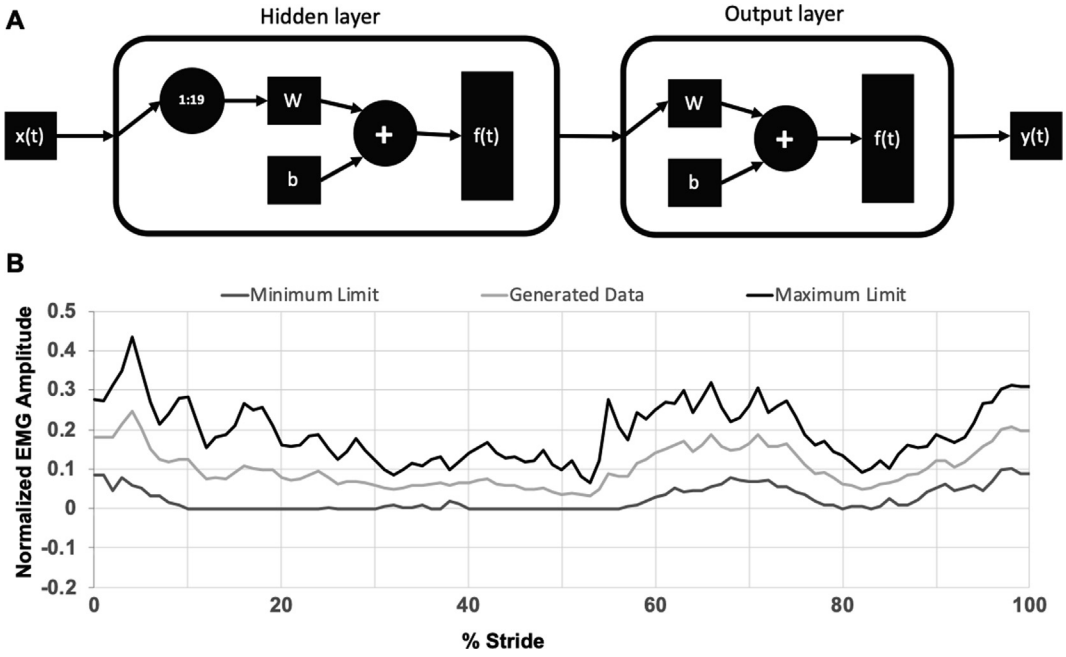

Fig. 1. NN structure and data generation for training. (A) A basic representation of the proposed NN structure. *x(t)* and *y(t)* represent the sEMG amplitude and, position and moment estimations as NN inputs and outputs, respectively. *f(t)* represents artificial neuron function specified for each layer (sigmoidal transfer function and linear transfer function in the hidden and output layer, respectively) in the NNs. (1:19) shows the nineteen-data-tapped delay in the hidden layer which has 32 neurons. Weight and bias of each neuron in the hidden and output layer are represented by *w* and *b*. (B) A sample normalized sEMG amplitude of the tibialis anterior (TA) muscle (medium speed, adult group): the maximum (black line), minimum (dark grey line) and a generated (light grey line) signal are shown.

Table 1
Training and test datasets for the main and versatility implementations.

Main Implementation	
Training Datasets	Test Dataset
Very slow, Slow, Medium and Fast speed classes	*Self-Selected speed class*
Versatility Implementations	
Training Datasets	Test Dataset
Slow, Medium, Self-selected and Fast speed classes	*Very slow speed class*
Very slow, Medium, Self-selected and Fast speed classes	*Slow speed class*
Very slow, Slow, Self-selected and Fast speed classes	*Medium speed class*
Very slow, Slow, Medium and Self-selected speed classes	*Fast speed class*

However, in order to increase the training efficiency and to avoid its inadequacy (even five muscle combination in main implementation yielded correlations <70% for both position and moment estimations), a protocol was devised for extending those and reproducing new training datasets. To do this, for each muscle input from each of the training dataset, three new ones were generated randomly, but by maintaining data distribution among the input and training datasets as bound by the minimum and maximum limits of data (Fig. 1B). Consequently, the total number of training datasets was increased to 32. Possible bias in correlation assessment due to such data augmentation was avoided by applying magnitude warping and noise adding techniques to sEMG data (Siu et al., 2018).

2.3.3. Training

Networks were trained in MATLAB by using Bayesian regularization backpropagation algorithm, which is a supervised learning method that requires known, desired outputs for each input. Backpropagation algorithm updates the weight and bias values of each neuron in a NN according to Levenberg-Marquardt optimization. The algorithm minimizes a linear combination of squared errors and weights and subsequently determines optimal parameters for a NN structure that generates the desired outputs (MacKay, 1992).

2.4. Evaluation of the developed neural networks

To evaluate the outcome of the developed NN variations for joint position and moment, the following were used: (1) Pearson's correlation coefficient (r) between the actual and estimated outputs was calculated and r = 0.95 was selected to represent the threshold for successful correlations (e.g., Chen et al., 2018). A *miscorrelation score* was defined as the sum of deviation of correlation values from one. (2) Root-mean-square errors (RMSE) between the actual and the estimated outputs were calculated. An *RMSE score* was defined as the mean of position and moment RMSE values normalized to their respective peak value among all variations. (3) An *overall error score* was defined as the product of miscorrelation and RMSE scores.

2.4.1. Main implementation

Using the overall error score, all variations were ranked and the economic and flexible variations were determined.

2.4.2. Versatility implementation

Normal Q-Q plots for the residuals between original data and NN response were used to illustrate if the residuals follow a normal distribution. One-way ANOVA was used for temporal success assessment based on one-dimensional statistical parametric mapping (SPM) using F-statistics (Pataky, 2010). Differences between the original data and estimated outputs were considered significant at $P < 0.05$.

Table 2
The comparison of the NN variations.

Variation	Position Correlation [r]	Moment Correlation [r]	Miscorrelation Score	Position RMSE (Deg)	Moment RMSE (Nm/kg)	RMSE Score	Overall Error Score
TA+MG+BF+RF+GM	0.987	0.995	0.018	1.388 ± 0.058	0.053 ± 0.016	0.166	0.0030
TA+MG+RF+BF	0.983	0.995	0.022	1.471 ± 0.339	0.040 ± 0.013	0.156	0.0034
TA+MG+RF+GM	0.980	0.997	0.023	1.466 ± 0.437	0.043 ± 0.010	0.160	0.0036
TA+MG+BF	0.981	0.996	0.024	1.537 ± 0.058	0.038 ± 0.007	0.159	0.0038
TA+MG+RF	0.978	0.994	0.028	1.510 ± 0.274	0.047 ± 0.028	0.168	0.0046
TA+MG+BF+GM	0.973	0.996	0.031	1.942 ± 0.053	0.042 ± 0.005	0.193	0.0060
TA+MG+GM	0.973	0.995	0.032	2.071 ± 0.497	0.052 ± 0.007	0.215	0.0068
MG+RF+BF+GM	0.974	0.991	0.035	1.843 ± 0.376	0.063 ± 0.026	0.212	0.0075
MG+BF+GM	0.955	0.995	0.050	2.251 ± 0.335	0.042 ± 0.005	0.215	0.0106
MG+RF+GM	0.960	0.994	0.046	2.466 ± 0.334	0.050 ± 0.000	0.240	0.0111
TA+MG	0.952	0.997	0.052	2.357 ± 0.150	0.041 ± 0.006	0.221	0.0115
MG+RF+BF	0.944	0.995	0.062	2.651 ± 0.220	0.051 ± 0.007	0.255	0.0157
MG+RF	0.907	0.995	0.097	3.472 ± 0.920	0.043 ± 0.008	0.304	0.0296
MG+BF	0.909	0.991	0.101	3.117 ± 1.435	0.063 ± 0.009	0.303	0.0305
TA+RF+BF+GM	0.954	0.941	0.104	2.266 ± 0.125	0.149 ± 0.047	0.351	0.0367
MG+GM	0.869	0.995	0.137	3.421 ± 0.322	0.043 ± 0.005	0.300	0.0411
TA+BF	0.935	0.934	0.130	2.461 ± 0.076	0.157 ± 0.009	0.376	0.0491
TA+RF+GM	0.954	0.919	0.127	2.372 ± 0.547	0.171 ± 0.054	0.387	0.0491
TA+RF+BF	0.942	0.921	0.137	2.635 ± 0.766	0.160 ± 0.031	0.392	0.0537
TA+BF+GM	0.933	0.927	0.141	2.466 ± 0.206	0.180 ± 0.045	0.406	0.0570
TA	0.921	0.923	0.156	2.926 ± 0.078	0.155 ± 0.041	0.406	0.0635
MG	0.821	0.993	0.186	3.931 ± 0.258	0.059 ± 0.001	0.357	0.0664
TA+RF	0.922	0.913	0.165	3.071 ± 1.049	0.176 ± 0.075	0.443	0.0734
TA+GM	0.909	0.868	0.222	3.053 ± 0.705	0.202 ± 0.066	0.476	0.1058
RF+BF	0.901	0.820	0.279	3.601 ± 2.008	0.264 ± 0.123	0.594	0.1656
RF+BF+GM	0.893	0.815	0.292	3.633 ± 0.460	0.250 ± 0.008	0.577	0.1685
RF+GM	0.750	0.594	0.656	5.162 ± 0.997	0.338 ± 0.042	0.799	0.5241
BF+GM	0.601	0.727	0.672	6.001 ± 1.072	0.304 ± 0.079	0.816	0.5486
RF	0.587	0.639	0.774	5.817 ± 0.471	0.325 ± 0.028	0.830	0.6423
BF	0.442	0.536	1.023	5.702 ± 0.322	0.374 ± 0.072	0.883	0.9031
GM	0.410	0.359	1.230	6.954 ± 0.492	0.395 ± 0.041	1.000	1.2302

Shaded cells show unsuccessful variations (i.e., r < 0.95). TA: tibialis anterior, MG: medial gastrocnemius, RF: rectus femoris, BF: biceps femoris, GM: gluteus maximus, RMSE: root-mean-square error.

Table 3
TA + MG + BF versatility per different implementation datasets.

Implementation Dataset	Position Correlation (r)	Moment Correlation (r)	Position RMSE [Deg]	Moment RMSE [Nm/kg]
Very Slow	0.986	0.998	1.31 ± 0.14	0.025 ± 0.00
Slow	0.965	0.995	2.07 ± 0.43	0.046 ± 0.03
Medium	0.971	0.985	2.30 ± 0.42	0.090 ± 0.00
Self-selected	0.981	0.996	1.54 ± 0.06	0.038 ± 0.01
Fast	0.990	0.997	1.13 ± 0.29	0.032 ± 0.00

TA: tibialis anterior, MG: medial gastrocnemius, BF: biceps femoris.

Table 4
MG + BF + GM versatility per different implementation datasets.

Implementation Dataset	Position Correlation (r)	Moment Correlation (r)	Position RMSE [Deg]	Moment RMSE [Nm/kg]
Very Slow	0.975	0.997	1.58 ± 0.14	0.035 ± 0.01
Slow	0.974	0.997	1.66 ± 0.43	0.035 ± 0.00
Medium	0.981	0.996	1.59 ± 0.21	0.037 ± 0.01
Self-selected	0.981	0.996	1.54 ± 0.06	0.038 ± 0.01
Fast	0.974	0.995	1.70 ± 0.48	0.039 ± 0.01

MG: medial gastrocnemius, BF: biceps femoris, GM: gluteus maximus.

3. Results

3.1. Main implementation

Table 2 shows correlation coefficients (see supplementary document for their visualization), miscorrelation scores, RMSE values, RMSE scores of all variations, and provides their ranking based on their overall error score.

The five muscle combination (TA + MG + BF + RF + GM) ranks 1st amongst all variations ($r_{position}$ and r_{moment} > 0.985).

Four muscle combinations: all variations show successful correlations ($r_{position}$ and r_{moment} > 0.973) except TA + RF + BF + GM.

Three muscle combinations: TA + MG + BF, TA + MG + RF, TA + MG + GM, MG + BF + GM and MG + RF + GM show successful correlations ($r_{position}$ and r_{moment} > 0.955). The remaining variations were unsuccessful.

Two muscle combinations show that only TA + MG ($r_{position}$ = 0.952, r_{moment} = 0.997) yields successful correlations whereas, no NN comprised of a single muscle shows successful correlations.

Therefore, the economic variation is TA + MG + BF ($r_{position}$ = 0.981, r_{moment} = 0.996). As all variations including only upper leg muscles were unsuccessful, no ideally flexible variation is possible, whereas the flexible variation is MG + BF + GM ($r_{position}$ = 0.955, r_{moment} = 0.995).

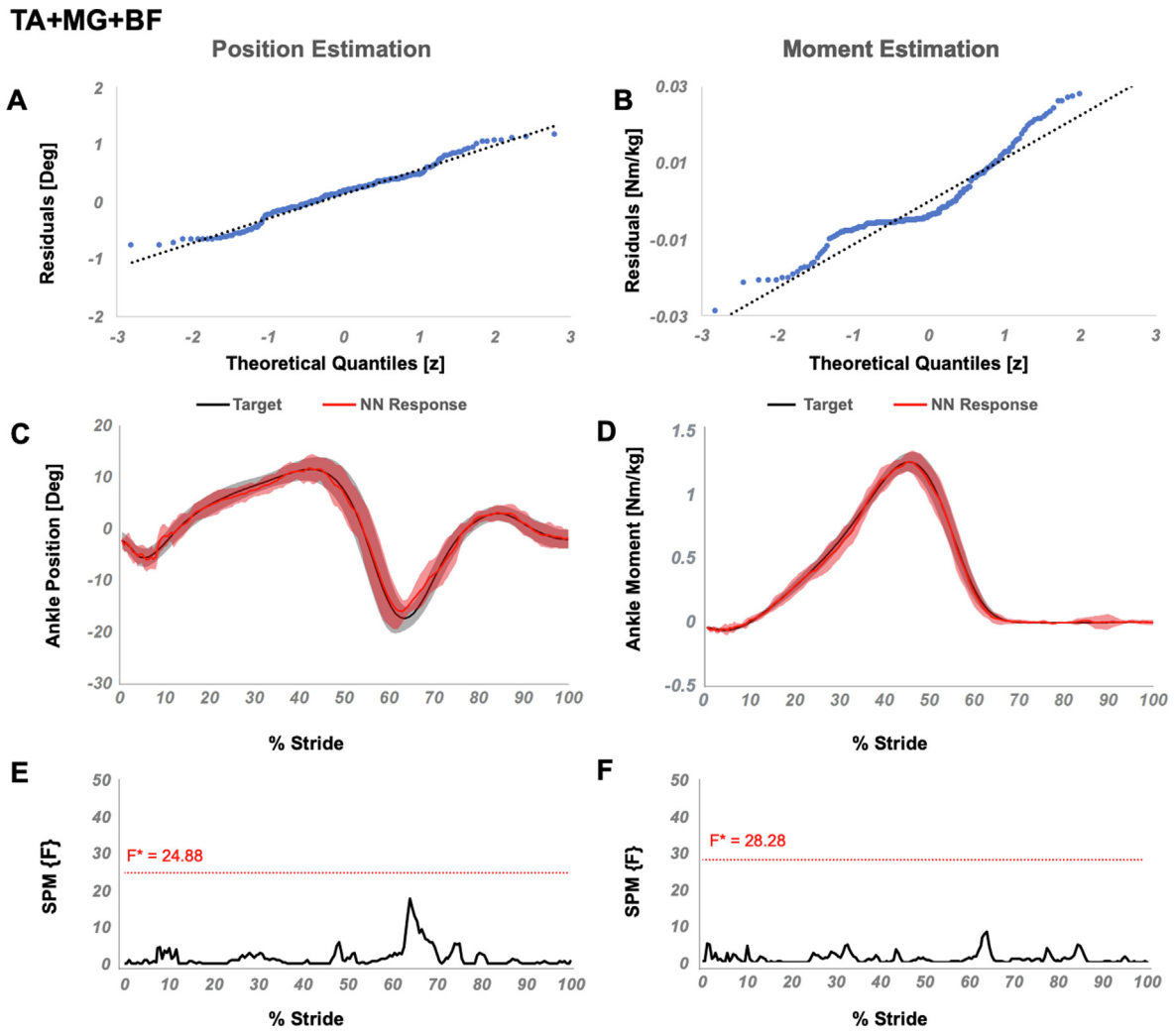

Fig. 2. Temporal success assessment for TA + MG + BF. The normal Q-Q plots for the residuals between original data and estimated NN response for ankle (A) position and (B) moment. Mean and standard deviation of estimated NN response vs. original data for ankle (C) position and (D) moment, as a function of % stride. Statistical parametric mapping using F-statistics (SPM{F}) for ankle (E) position and (F) moment as a function of % stride shows values below the threshold (i.e., for P < 0.05, $F^*_{position}$ = 24.88, F^*_{moment} = 28.28). TA abbreviates tibialis anterior, MG abbreviates medial gastrocnemius and BF abbreviates biceps femoris muscles.

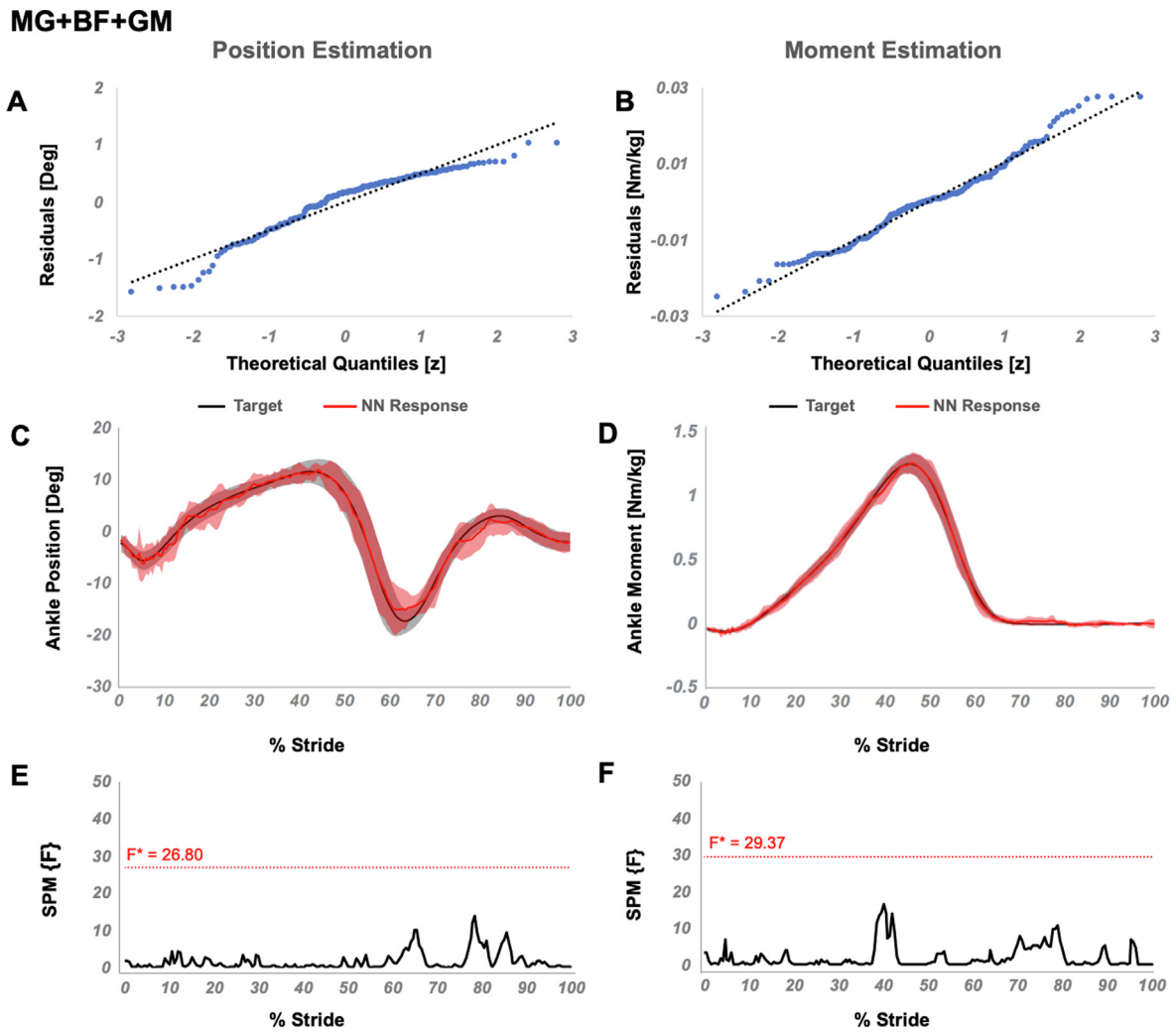

Fig. 3. Temporal success assessment for MG + BF + GM. The normal Q-Q plots for the residuals between original data and estimated neural NN response for ankle (A) position and (B) moment. Mean and standard deviation of estimated NN response vs. original data for ankle (C) position and (D) moment, as a function of % stride. Statistical parametric mapping using F-statistics (SPM{F}) for ankle (E) position and (F) moment as a function of % stride shows values below the threshold (i.e., for $P < 0.05$, $F^*_{position} = 26.80$, $F^*_{moment} = 29.37$). MG abbreviates medial gastrocnemius, BF abbreviates biceps femoris and GM abbreviates gluteus maximum muscles.

3.2. Versatility implementation

TA + MG + BF and MG + BF + GM were able to produce estimation correlations above 0.950 for both position and moment (Table 3 and 4, respectively) after being subject to implementation of very slow, slow, medium and fast speed classes. SPM showed no significant localized differences between the actual and estimated outputs for both TA + MG + BF (Fig. 2) and MG + BF + GM (Fig. 3).

4. Discussion

Souza et al. (2014) argued that the evolution of motorized knee and ankle components of powered prostheses has introduced a need for more advanced approaches to achieve prosthetic control. They also indicated that although myoelectric control schemes can be applied to the lower extremity, they must be merged with mechanical and timing-based control methods in order to achieve seamless and natural ambulation. Within this scope, on contrary to the standard multilayer feedforward NN approach, Rahmatian et al. (2016) showed that by using time delay feed-forward multilayer NN with sEMG inputs collected from TA, MG and lateral gastrocnemius muscles, the intended motion of a subject can be estimated. Although the detection of the ankle movements was not aimed at, that study showed that an accurate sEMG classification for the estimation of the ankle movement is plausible by using a shift-invariant classification. Also, Liu et al. (2017) was able to achieve an sEMG-based continuous and simultaneous estimation of arm kinematics in able-bodied individuals and stroke survivors by using this type of NN. Based on such earlier indicated promise of that approach, a time delay feed-forward multilayer NN architecture that produces outputs using sequential inputs was implemented in the present study. The NNs developed have 32 neurons with a nineteen-data-tapped delay in their hidden layer, which allows accurate ankle movement estimations. Unlike previous studies (Au et al., 2008; Fleischer and Hommel, 2008; Kiguchi and Hayashi, 2012; Sup et al., 2008), the developed NN structure is capable of providing ankle movement estimations without the need of an extra mathematical model, a supportive NN or a force feedback implementation. Note that achieving 0.95 correlation in ankle position estimation, Chen et al. (2018) reported an RMSE of 2.45°, and for 0.97 correlation in ankle moment estimation, Hahn and O'Keefe (2008) reported an RMSE of 0.10 Nm/kg. However,

they utilized 7–10 muscles. Utilizing only three muscles, our present algorithm yields 1.53° and 0.04 Nm/kg RMSE for over 0.98 correlation in position and moment estimations indicating compatible or improved success compared to previous studies.

A key use of sEMG amplitudes in the development of the powered prosthesis is to pre-determine the movement of the ankle during level ground walking. Bovi et al. (2011) showed for different walking types that lower extremity muscles generate specific and consistent sEMG patterns in each gait cycle. Additionally, Huang and Ferris (2012) showed that sEMG amplitudes of also upper leg muscles in transtibial amputations are consistent. They used sEMG of the residual limb muscles within the prosthetic socket-limb interface as collected by surface electrodes. Their results support the potential use of myoelectric controllers for direct feed-forward control of powered prostheses. Consequently, sEMG was proven useful as control inputs for powered prostheses for an accurate prediction of the intended joint motion in terms of position and moment changes. However, elaboration on which muscles are to be utilized has been lacking. Au et al. (2008, 2005) used TA, soleus, MG and lateral gastrocnemius muscles not only to estimate ankle movements in transtibial amputations, but also to detect the locomotion task. Fleischer and Hommel (2008) used RF, vastus medialis, vastus lateralis, semimembranosus, semitendinosus, and BF muscles to control a powered leg exoskeleton. Zhang et al. (2010) designed a feed-forward NN model to control an ankle exoskeleton using sEMG amplitudes from TA, MG, soleus, lateral gastrocnemius and peroneus longus muscles. Huang et al. (2011) used sEMG amplitudes from sartorius, RF, vastus lateralis, vastus medialis, gracilis, biceps femoris long head, semitendinosus, biceps femoris short head and adductor magnus to recognize locomotion modes for transfemoral amputees. Hargrove et al. (2015) used semitendinosus, BF, tensor fascia*e* latae, RF, vastus lateralis, vastus medialis, sartorius, adductor magnus and gracilis to control a powered knee-ankle prosthetics. Spanias et al. (2018) developed an intent recognition algorithm for a powered knee/ankle prosthesis using sEMG amplitudes collected from RF, tensor fascia*e* latae, semitendinosus and adductor magnus. Nevertheless, none of those studies provided a specific reason other than their being activated during walking nor did a systematic analysis for the selection of the targeted muscles to be used as control inputs for their systems. Presently, possible combinations of TA and MG muscles in the lower leg and RF, BF and GM muscles in the upper leg were studied comprehensively. Note that despite its key role in ankle movement, collecting accurate sEMG data from the soleus can be problematic using surface electrodes. Hence, this muscle was excluded, which agrees with Huang and Ferris (2012). Those authors showed that the use of TA, MG, lateral gastrocnemius, vastus lateralis, RF, BF, and gluteus muscles' myoelectric signals provide successful control for robotic lower limb prostheses.

The present study shows the feasibility of the time delay feed-forward NNs for predicting ankle angle and moment using exclusively sEMG amplitudes for level walking of a healthy population. For the sake of minimizing the use of sEMG muscle sources it is notable that TA + MG combination alone yields successful correlations. The assessment showed that the *economic* variation i.e., the best-performing NN including the minimum total number of muscle inputs (TA + MG + BF) also involves those muscles. Another important finding is that the use of solely upper leg muscles is not feasible. However, successful three muscle combinations involving only the GM were shown, with the *flexible* variation to minimize the number of lower leg muscles was determined as MG + BF + GM. Although the present findings are not directly transferrable to people with amputations or disease, they suggest that plausible NN variations exist for ankle disarticulation, confirmation of which requires specific studies. Yet, they also suggest that for a NN approach using exclusively sEMG amplitudes, involvement of lower leg muscles is inevitable for transtibial amputation. Note that, Huang and Ferris (2012) showed in transtibial amputees that artifact-free and consistent sEMG can be recorded from lower leg muscles within the prosthetic socket-limb interface. However, in the long-term use, walking with electrodes beneath the socket can compromise the comfort for persons with limb amputation, and the repeated application of electrodes can affect the sensor lifetime adversely. Use of e.g., sEMG knit band sensor (Lee et al., 2018) can make implementation much easier and may help compromised comfort. On the other hand, high-density sEMG can help avoiding problems related with bipolar sEMG electrode placement and signals (Ison et al., 2016), and improve data quality (Rojas-Martínez et al., 2012; Zwarts and Stegeman, 2003). Clites et al. (2018) and Srinivasan et al. (2019) showed that surgically constructed agonist-antagonist myoneural interfaces in the residual limb serve efficiently on torque-controlled tasks. This is promising for conceivable restoration of natural sensation to prosthetic joints, but targeted muscle re-innervation should be accounted for.

Commercially available powered ankle-foot prosthesis controllers are rare and improving the function in amputees is challenging. A neuromuscular model based controller utilized in bionic ankle-foot prosthesis (Herr and Grabowski, 2012) is capable of normalizing gait during level walking for amputees. A bio-inspired control algorithm has recently been proposed to provide adaptive control of level walking and stair ascent (Tahir et al., 2018). However, utilization of the provided power by the users with transtibial amputation, in a way to reduce the metabolic cost of motion requires care (Ingraham et al., 2018). In addition, uphill and downhill walking as well as stair ascent/descent movements not only require more power (Jeffers and Grabowski, 2017; Wilken et al., 2011), but also an improved leg work symmetry, and control over the contributions of ankle, knee and hip joint work needs to be achieved (Montgomery and Grabowski, 2018a, 2018b). Therefore, more and systematic work is necessary to improve powered ankle-foot prosthesis controllers. The present study aims at contributing to that and with a neural network approach using sEMG as the sensor source, which requires additional studies and testing in amputees. Note that, the overall error score we used for ranking combines miscorrelation and RMSE between the actual and the estimated outputs into a single metric and takes ankle position and moment errors into account being equally weighted. This is suitable for our aim of testing of the feasibility of the algorithms in the present development study conducted in a healthy population. However, uphill/downhill walking and stair ascent/descent movements and mobility of amputees may require differential weighting, which also needs to be studied.

Limitations of the developed methodology need to be addressed. Presently the NN structures developed and tested remain in reference to healthy individuals only. The open database by Bovi et al. (2011) involving suitably processed sEMG data of various muscles is very useful and is a rarity. However, although for level ground walking a sufficient number of data sets were available for NN training and implementation, this was limited to only two for toe-walking, heel-walking, step ascending and step descending. Therefore, the NN based control algorithm needs to be extended by the estimation of the intended movement after it is re-trained with sufficient number of datasets for different locomotion tasks. The lack of an open database that consists of data of amputees limits further testing of the control algorithm developed. One plausible source of inconsistency is that the size of the residual limb, hence the volume of the lower leg muscles may differ across amputees. This hinders the use of a standard sEMG sensor placement, which yielded a low cross-correlation between

sEMG patterns of transtibial amputees and controls particularly for the BF (Huang and Ferris, 2012). However, after determining suitable electrode locations using palpation, the authors successfully measured sEMG of TA, MG and lateral gastrocnemius and four upper leg muscles of transtibial amputees during walking and reported that they were able to voluntarily activate their residual lower leg muscles with several of them producing activation profiles similar to healthy controls. Training their control algorithm using sEMG of lateral gastrocnemius, MG and TA in bilateral transtibial amputees, Au et al. (2008) achieved ankle position and moment patterns comparable to those of a healthy subject during level ground walking. Similarly, Huang et al. (2011) reported highly accurate powered prosthesis control by using sEMG of nine residual limb muscles of transfemoral amputees including the BF. The presently best-performing variation, TA + MG + BF may not therefore be prone to significant implementation problems, but this needs to be tested. However, the use of normalized sEMG data may bear difficulties for practical applicability in a real system, which imposes a major time limitation for the required computation. Yet, competent use of non-normalized sEMG in joint position and moment estimation has been reported e.g., in upper-limb amputees (Hudgins et al., 1993). Huang et al.'s (2011) ankle movement estimation accuracy using non-normalized sEMG is comparable to our present findings. This is promising and limiting of the preprocessing to bandpass filtering and rectification (Au et al., 2008) is a more practical alternative. Overall, accuracy of ankle movement estimations should be studied after re-training the developed control algorithm with a large database including non-normalized sEMG data collected from lower extremity amputees.

In summary, a novel NN approach utilizing exclusively lower limb sEMG was developed. Its feasibility for predicting ankle angle and moment during level walking of a healthy population was evaluated comprehensively by testing all muscle combinations among TA, GM, RF, BF and MG muscles. NN variations TA + MG + BF and MG + BF + GM showed the best predictive performances while minimizing the total number of muscle sEMG sources and minimizing the use of lower leg muscles, respectively. Following further development, this approach can be applicable in powered ankle prosthesis control algorithms. For this purpose, after extending their implementation with other movement types, the algorithms should be trained and tested for data acquired from amputees in new studies.

Declaration of Competing Interest

The authors declare that they have no known competing financial interests or personal relationships that could have appeared to influence the work reported in this paper.

Acknowledgements

We thank Cemre Su Kaya for her helps in statistical analyses.

Appendix A. Supplementary material

Supplementary data to this article can be found online at https://doi.org/10.1016/j.jbiomech.2020.110087.

References

Al-Quraishi, M.S., Ishak, A.J., Ahmad, S.A., Hasan, M.K., 2015. Impact of feature extraction techniques on classification accuracy for EMG based ankle joint movements. In: 2015 10th Asian Control Conference: Emerging Control Techniques for a Sustainable World, ASCC 2015. https://doi.org/10.1109/ASCC.2015.7244844.

Au, S., Berniker, M., Herr, H., 2008. Powered ankle-foot prosthesis to assist level-ground and stair-descent gaits. Neural Networks 21, 654–666. https://doi.org/10.1016/j.neunet.2008.03.006.

Au, S.K., Bonato, P., Herr, H., 2005. An EMG-position controlled system for an active ankle-foot prosthesis: An initial experimental study. In: Proceedings of the 2005 IEEE 9th International Conference on Rehabilitation Robotics. https://doi.org/10.1109/ICORR.2005.1501123.

Bovi, G., Rabuffetti, M., Mazzoleni, P., Ferrarin, M., 2011. A multiple-task gait analysis approach: Kinematic, kinetic and EMG reference data for healthy young and adult subjects. Gait Posture 33, 6–13. https://doi.org/10.1016/j.gaitpost.2010.08.009.

Cavallaro, E.E., Rosen, J., Perry, J.C., Burns, S., 2006. Real-time myoprocessors for a neural controlled powered exoskeleton arm. IEEE Trans. Biomed. Eng. 53, 2387–2396. https://doi.org/10.1109/TBME.2006.880883.

Chen, J., Zhang, X., Cheng, Y.u., Xi, N., 2018. Surface EMG based continuous estimation of human lower limb joint angles by using deep belief networks. Biomed. Signal Process. Control 40, 335–342. https://doi.org/10.1016/j.bspc.2017.10.002.

Clites, T.R., Carty, M.J., Ullauri, J.B., Carney, M.E., Mooney, L.M., Duval, J.-F., Srinivasan, S.S., Herr, H.M., 2018. Proprioception from a neurally controlled lower-extremity prosthesis. Sci. Transl. Med. 10. https://doi.org/10.1126/scitranslmed.aap8373.

Culver, S., Bartlett, H., Shultz, A., Goldfarb, M., 2018. A stair ascent and descent controller for a powered ankle prosthesis. IEEE Trans. Neural Syst. Rehabil. Eng. 26, 993–1002. https://doi.org/10.1109/TNSRE.2018.2819508.

De Luca, C.J., Donald Gilmore, L., Kuznetsov, M., Roy, S.H., 2010. Filtering the surface EMG signal: movement artifact and baseline noise contamination. J. Biomech. 43, 1573–1579. https://doi.org/10.1016/j.jbiomech.2010.01.027.

Fleischer, C., Hommel, G., 2008. A human–exoskeleton interface utilizing electromyography. IEEE Trans. Robot. 24 (4), 872–882. https://doi.org/10.1109/TRO.2008.926860.

Gates, D.H., Lelas, J., Della Croce, U., Herr, H., Bonato, P., 2004. Characterization of ankle function during stair ambulation. IEEE Eng. Med. Biol. – Proc., 4248–4251 https://doi.org/10.1109/iembs.2004.1404184.

Hahn, M.E., O'Keefe, K.B., 2008. A neural network model for estimation of net joint moments during normal gait. J. Musculoskelet. Res. 11, 117–126. https://doi.org/10.1142/S0218957708002036.

Hargrove, L.J., Young, A.J., Simon, A.M., Fey, N.P., Lipschutz, R.D., Finucane, S.B., Halsne, E.G., Ingraham, K.A., Kuiken, T.A., 2015. Intuitive control of a powered prosthetic leg during ambulation: a randomized clinical trial. JAMA 313, 2244. https://doi.org/10.1001/jama.2015.4527.

Hermens, H.J., Freriks, B., Disselhorst-Klug, C., Rau, G., 2000. Development of recommendations for SEMG sensors and sensor placement procedures. J. Electromyography Kinesiol. 10, 361–374. https://doi.org/10.1016/S1050-6411(00)00027-4.

Herr, H.M., Grabowski, A.M., 2012. Bionic ankle–foot prosthesis normalizes walking gait for persons with leg amputation. Proc. R. Soc. B. 279 (1728), 457–464. https://doi.org/10.1098/rspb.2011.1194.

Hoozemans, M.J.M., van Dieën, J.H., 2005. Prediction of handgrip forces using surface EMG of forearm muscles. J. Electromyography Kinesiol. 15 (4), 358–366. https://doi.org/10.1016/j.jelekin.2004.09.001.

Huang, H., Zhang, F., Hargrove, L.J., Dou, Z., Rogers, D.R., Englehart, K.B., 2011. Continuous locomotion-mode identification for prosthetic legs based on neuromuscular – mechanical fusion. IEEE Trans. Biomed. Eng. 58, 2867–2875. https://doi.org/10.1109/TBME.2011.2161671.

Huang, S., Ferris, D.P., 2012. Muscle activation patterns during walking from transtibial amputees recorded within the residual limb-prosthetic interface. J. NeuroEngineering Rehabil. 9, 55. https://doi.org/10.1186/1743-0003-9-55.

Hudgins, B., Parker, P., Scott, R.N., 1993. A new strategy for multifunction myoelectric control. IEEE Trans. Biomed. Eng. 40, 82–94. https://doi.org/10.1109/10.204774.

Ingraham, K.A., Choi, H., Gardinier, E.S., Remy, C.D., Gates, D.H., 2018. Choosing appropriate prosthetic ankle work to reduce the metabolic cost of individuals with transtibial amputation. Sci Rep 8. https://doi.org/10.1038/s41598-018-33569-7.

Ison, M., Vujaklija, I., Whitsell, B., Farina, D., Artemiadis, P., 2016. High-Density electromyography and motor skill learning for robust long-term control of a 7-DoF robot arm. IEEE Trans. Neural Syst. Rehabil. Eng. 24, 424–433. https://doi.org/10.1109/TNSRE.2015.2417775.

Jeffers, J.R., Grabowski, A.M., 2017. Individual leg and joint work during sloped walking for people with a transtibial amputation using passive and powered prostheses. Front. Robot. AI. https://doi.org/10.3389/frobt.2017.00072.

Jephil, P.B., Acharaya, P., Xu, L., Guo, K., Yu, H., Watsford, M., Rong, S., Su, S., 2020. Estimation of Ankle Joint Torque and Angle Based on S-EMG Signal for Assistive Rehabilitation Robots. In: Naik, G. (Ed.), Biomedical Signal Processing. Series in BioEngineering. Springer, Singapore. https://doi.org/10.1007/978-981-13-9097-5_2.

Kiguchi, K., Hayashi, Y., 2012. An EMG-based control for an upper-limb power-assist exoskeleton robot. IEEE Trans. Syst., Man, Cybern. B 42, 1064–1071. https://doi.org/10.1109/TSMCB.2012.2185843.

Lawson, B.E., Mitchell, J., Truex, D., Shultz, A., Ledoux, E., Goldfarb, M., 2014. A robotic leg prosthesis: design, control, and implementation. IEEE Robot. Automat. Mag. 21, 70–81. https://doi.org/10.1109/MRA.2014.2360303.

Lee, S., Kim, M.-O., Kang, T., Park, J., Choi, Y., 2018. Knit band sensor for myoelectric control of surface EMG-based prosthetic hand. IEEE Sensors J. 18, 8578–8586. https://doi.org/10.1109/JSEN.2018.2865623.

Lencioni, T., Carpinella, I., Rabuffetti, M., Marzegan, A., Ferrarin, M., 2019. Human kinematic, kinetic and EMG data during different walking and stair ascending and descending tasks. Sci Data 6. https://doi.org/10.1038/s41597-019-0323-z.

Liu, J., Kang, S.H., Xu, D., Ren, Y., Lee, S.J., Zhang, L.Q., 2017. EMG-Based continuous and simultaneous estimation of arm kinematics in able-bodied individuals and stroke survivors. Front. Neurosci. 11, 480. https://doi.org/10.3389/fnins.2017.00480.

MacKay, D.J.C., 1992. A practical Bayesian framework for backpropagation networks. Neural Comput. 4, 448–472. https://doi.org/10.1162/neco.1992.4.3.448.

Montgomery, J.R., Grabowski, A.M., 2018a. Use of a powered ankle–foot prosthesis reduces the metabolic cost of uphill walking and improves leg work symmetry in people with transtibial amputations. J. R. Soc. Interface:, 20180442. https://doi.org/10.1098/rsif.2018.0442.

Montgomery, J.R., Grabowski, A.M., 2018b. The contributions of ankle, knee and hip joint work to individual leg work change during uphill and downhill walking over a range of speeds. R. Soc. Open Sci. https://doi.org/10.1098/rsos.180550.

Naidu, D.S., Chen, C.H., Perez, A., Schoen, M.P., 2008. Control strategies for smart prosthetic hand technology: an overview. In: Proceedings of the 30th Annual International Conference of the IEEE Engineering in Medicine and Biology Society, pp. 4314–4317. https://doi.org/10.1109/iembs.2008.4650164.

Palmer, M.L., 2002. Sagittal plane charactrization of normal human ankle function across a range of walking gait speeds. Massachusetts Inst. Technol.

Pataky, T.C., 2010. Generalized n-dimensional biomechanical field analysis using statistical parametric mapping. J. Biomech. 43, 1976–1982. https://doi.org/10.1016/j.jbiomech.2010.03.008.

Pulliam, C.L., Lambrecht, J.M., Kirsch, R.F., 2011. Electromyogram-based neural network control of transhumeral prostheses. JRRD 48, 739. https://doi.org/10.1682/JRRD.2010.12.0237.

Rahmatian, S., Mahjoob, M.J., Hanachi, M.R., 2016. Continuous estimation of ankle joint angular position based on the myoelectric signals. In: 2016 Artificial Intelligence and Robotics, IRANOPEN 2016. pp. 158–163. https://doi.org/10.1109/RIOS.2016.7529507.

Rojas-Martínez, M., Mañanas, M.A., Alonso, J.F., 2012. High-density surface EMG maps from upper-arm and forearm muscles. J. NeuroEngineering Rehabil. https://doi.org/10.1186/1743-0003-9-85.

Sepulveda, F., Wells, D.M., Vaughan, C.L., 1993. A neural network representation of electromyography and joint dynamics in human gait. J. Biomech. 26, 101–109. https://doi.org/10.1016/0021-9290(93)90041-C.

Siu, W.-C., Chau, L.-P., Wang, L., Tang, T., 2018. Learning Approaches in Signal Processing. Pan Stanford Publishing.

Souza, J.M., Fey, N.P., Cheesborough, J.E., Agnew, S.P., Hargrove, L.J., Dumanian, G.A., 2014. Advances in transfemoral amputee rehabilitation: early experience with targeted muscle reinnervation. Curr Surg Rep 2, 51. https://doi.org/10.1007/s40137-014-0051-4.

Spanias, J.A., Simon, A.M., Finucane, S.B., Perreault, E.J., Hargrove, L.J., 2018. Online adaptive neural control of a robotic lower limb prosthesis. J. Neural Eng. 15, 016015. https://doi.org/10.1088/1741-2552/aa92a8.

Spanias, J.A., Simon, A.M., Ingraham, K.A., Hargrove, L.J., 2015. Effect of additional mechanical sensor data on an EMG-based pattern recognition system for a powered leg prosthesis. In: International IEEE/EMBS Conference on Neural Engineering. https://doi.org/10.1109/NER.2015.7146704.

Srinivasan, S.S., Diaz, M., Carty, M., Herr, H.M., 2019. Towards functional restoration for persons with limb amputation: a dual-stage implementation of regenerative agonist-antagonist myoneural interfaces. Sci. Rep. 9, 1–10. https://doi.org/10.1038/s41598-018-38096-z.

Sup, F., Varol, H.A., Mitchell, J., Withrow, T., Goldfarb, M., 2008. Design and control of an active electrical knee and ankle prosthesis. In: Proceedings of the 2nd Biennial IEEE/RAS-EMBS International Conference on Biomedical Robotics and Biomechatronics, BioRob 2008. pp. 523–528. https://doi.org/10.1109/BIOROB.2008.4762811.

Tahir, U., Hessel, A.L., Lockwood, E.R., Tester, J.T., Han, Z., Rivera, D.J., Covey, K.L., Huck, T.G., Rice, N.A., Nishikawa, K.C., 2018. Case study: A bio-inspired control algorithm for a robotic foot-ankle prosthesis provides adaptive control of level walking and stair ascent. Front. Robot. AI. https://doi.org/10.3389/frobt.2018.00036.

Tucker, M.R., Olivier, J., Pagel, A., Bleuler, H., Bouri, M., Lambercy, O., Millán, J.D.R., Riener, R., Vallery, H., Gassert, R., 2015. Control strategies for active lower extremity prosthetics and orthotics: a review. J NeuroEngineering Rehabil 12, 1. https://doi.org/10.1186/1743-0003-12-1.

Wilken, J.M., Sinitski, E.H., Bagg, E.A., 2011. The role of lower extremity joint powers in successful stair ambulation. Gait Posture 34. https://doi.org/10.1016/j.gaitpost.2011.03.015.

Zhang, Z., Jiang, J., Peng, L., Fan, H., 2010. A method to control ankle exoskeleton with surface electromyography signals. In: International Conference on Intelligent Robotics and Applications ICIRA 2010: Intelligent Robotics and Applications, pp. 390–397. https://doi.org/10.1007/978-3-642-16587-0_36.

Zwarts, M.J., Stegeman, D.F., 2003. Multichannel surface EMG: Basic aspects and clinical utility. Muscle Nerve 28 (1), 1–17.